Catalysis Today 145 (2009) 267–278

Contents lists available at ScienceDirect

Catalysis Today

journal homepage: www.elsevier.com/locate/cattod

Catalysts at work: From integral to spatially resolved X-ray absorption spectroscopy

Jan-Dierk Grunwaldt [a,*], Bertram Kimmerle [b], Alfons Baiker [b], Pit Boye [c], Christian G. Schroer [c], Pieter Glatzel [d], Camelia N. Borca [e], Felix Beckmann [f]

[a] Department of Chemical and Biochemical Engineering, Technical University of Denmark, DK-2800 Kgs. Lyngby, Denmark
[b] Institute for Chemical and Bioengineering, Department of Chemistry and Applied Biosciences, ETH Zurich, Hönggerberg – HCI, CH-8093 Zurich, Switzerland
[c] Institute of Structural Physics, Technische Universität Dresden, D-01062 Dresden, Germany
[d] European Synchrotron Radiation Facility (ESRF), BP220, 6 rue Jules Horowitz, F-38043 Grenoble, France
[e] Swiss Light Source, Paul-Scherrer Institut, CH-5232 Villigen, Switzerland
[f] Institute for Materials Research, GKSS Research Center, Max-Planck-Str. 1, D-21502 Geesthacht, Germany

ARTICLE INFO

Article history:
Available online 19 December 2008

Keywords:
Spatially resolved spectroscopy
X-ray microscopy
In situ spectroscopy
X-ray absorption spectroscopy
Partial oxidation of methane
Tomography

ABSTRACT

Spectroscopic studies on heterogeneous catalysts have mostly been done in an integral mode. However, in many cases spatial variations in catalyst structure can occur, e.g. during impregnation of pre-shaped particles, during reaction in a catalytic reactor, or in microstructured reactors as the present overview shows. Therefore, spatially resolved molecular information on a microscale is required for a comprehensive understanding of theses systems, partly in *ex situ* studies, partly under stationary reaction conditions and in some cases even under dynamic reaction conditions.

Among the different available techniques, X-ray absorption spectroscopy (XAS) is a well-suited tool for this purpose as the different selected examples highlight. Two different techniques, scanning and full-field X-ray microscopy/tomography, are described and compared. At first, the tomographic structure of impregnated alumina pellets is presented using full-field transmission microtomography and compared to the results obtained with a scanning X-ray microbeam technique to analyse the catalyst bed inside a catalytic quartz glass reactor. On the other hand, by using XAS in scanning microtomography, the structure and the distribution of Cu(0), Cu(I), Cu(II) species in a Cu/ZnO catalyst loaded in a quartz capillary microreactor could be reconstructed quantitatively on a virtual section through the reactor. An illustrating example for spatially resolved XAS under reaction conditions is the partial oxidation of methane over noble metal-based catalysts. In order to obtain spectroscopic information on the spatial variation of the oxidation state of the catalyst inside the reactor XAS spectra were recorded by scanning with a micro-focussed beam along the catalyst bed. Alternatively, full-field transmission imaging was used to efficiently determine the distribution of the oxidation state of a catalyst inside a reactor under reaction conditions. The new technical approaches together with quantitative data analysis and an appropriate *in situ* catalytic experiment allowed drawing important conclusions on the reaction mechanism, and the analytical strategy might be similarly applied in other case studies. The corresponding temperature profiles and the catalytic performance were measured by means of an IR-camera and mass spectrometric analysis. In a more advanced experiment the ignition process of the partial oxidation of methane was followed in a spatiotemporal manner which demonstrates that spatially resolved spectroscopic information can even be obtained in the subsecond scale.

1. Introduction

X-ray-based techniques have played an important role over the past two decades in shedding light onto the structure of heterogeneous catalysts especially by means of X-ray diffraction (XRD), X-ray absorption spectroscopy (XAS) and small-angle X-ray scattering (SAXS) [1–5]. The big advantage of X-rays is that the structural information can be elucidated under reaction conditions and in a time-resolved manner [3,6–10], thus being an important technique within the toolbox of *in situ* spectroscopic methods [11,12]. Furthermore, XAS is very powerful regarding the often amorphous structures of heterogeneous catalysts and in uncovering the structure of elements at low concentration, such as noble metals, promoters and catalyst poisons.

* Corresponding author. Tel.: +45 4525 2838.
E-mail address: jdg@kt.dtu.dk (J.-D. Grunwaldt).

0920-5861/$ – see front matter © 2008 Elsevier B.V. All rights reserved.
doi:10.1016/j.cattod.2008.11.002

Many of these studies were performed in an integral manner, meaning that the sample was either crushed and pressed in the form of a pellet, even if the sample is usually present as pre-shaped particles (e.g. shell-impregnated cylinders, spheres), or it implies that the sample was measured over the whole reactor. However, catalysts are often microstructured by intention (shell-impregnation to improve the efficiency of the catalyst) which requires spatially resolved studies [13,14]. Besides, gradients in structure can occur over the catalyst bed due to temperature inhomogeneities (e.g. hot spots) or concentration gradients of the reactants/products [15–23].

In order to uncover such structural changes over the catalyst bed or inside the catalyst particles, several techniques can be used, e.g. scanning electron microscopy [24,25], micro-XRD [26], micro-IR [14,27,28], micro-Raman [23,29–31], and UV–vis spectroscopy [14] as well as NMR tomography [32,33]. Again, the advantage is the X-rays' ability to penetrate the sample and if an X-ray camera or a micro-focussed X-ray beam are used, they can give spatially resolved information non-invasively and even under process conditions.

In this overview article we stress the importance and the possibilities of spatially resolved spectroscopy in catalysis research by highlighting different examples from our research together with that of other groups in the field of catalyst preparation and *in situ* studies. Two different strategies to obtain spatially resolved information are discussed: scanning X-ray microscopy with a micro-focussed X-ray beam and full-field X-ray microscopy with an X-ray camera. They both have their own strengths as the different selected examples show. We start with examples of the shell-impregnation of solid catalysts using full-field X-ray microtomography and X-ray scanning microscopy to identify the metallic species in the pre-shaped particles and/or the catalyst bed. Then, scanning X-ray absorption tomography for quantitative identification of the distribution of Cu(0), Cu(I) and Cu(II) in a catalyst bed under *ex situ* conditions is discussed before moving eventually towards spatially resolved *in situ* studies. The challenges of the two techniques are discussed using the catalytic partial oxidation of methane over noble metal catalysts as an example. Finally, further opportunities such as spatiotemporal studies combined with temperature measurements of the catalytic reactor and high throughput experimentation are considered.

2. Imaging using X-ray-based microscopy and microtomography

One of the key strengths of X-ray imaging is the large penetration depth of hard X-rays in matter, allowing the non-destructive imaging of the interior of a sample inside a special sample environment, such as a catalytic reactor. There are mainly two X-ray microscopy techniques, full-field and scanning microscopy [19,34–38]. While full-field microscopy yields full transmission images of the sample in a single exposure, scanning microscopy allows the use of different X-ray analytical techniques, such as X-ray fluorescence, absorption, and diffraction, in order to obtain local elemental, chemical, and nanostructural information of the sample. Both techniques can be combined with X-ray absorption spectroscopy and are thus well suited for *operando* investigations of catalytic reactions inside a chemical reactor. Fig. 1 illustrates the principle of X-ray absorption spectroscopic imaging.

Scanning microscopy combined with absorption spectroscopy is shown in Fig. 1(a). In this technique, the sample is scanned with an intensive hard X-ray microbeam; a full X-ray absorption spectrum along the path of the beam through the sample is recorded at each position of the scan. This technique is described in detail in Section 4, where it is used to obtain the oxidation states of a Cu/Zn-oxide catalyst on a virtual section through a catalytic reactor.

Fig. 1(b) shows the full-field imaging scheme. The sample is illuminated with a flat monochromatic hard X-ray beam and its transmission image is recorded with a high-resolution X-ray camera. By recording a series of images at different energies over an absorption edge of a given element a full X-ray absorption spectrum can be obtained for each pixel.

In order to obtain quantitative transmission data from such images, a series of flat-field images (without the sample) has to be recorded to characterize the incident beam on the sample. The influence of the detector is removed by subtracting dark-field images (taken with the X-ray beam turned off) from both the transmission and flat-field images. In this way, the intensities in the transmission image $I(x, y)$ and in the flat-field image $I_0(x, y)$ are obtained for each pixel with coordinates (x, y). By applying Beer–Lambert's law the integral of the attenuation coefficient $\mu(x, y, z)$ along the beam (z-direction) is obtained for each (x, y) by taking the negative logarithm of the ratio of $I(x, y)$ and $I_0(x, y)$. The spatial resolution of this technique is limited by that of the detector and typically lies in the micrometer range. Higher spatial resolution, i.e. down to below 100 nm, can be obtained by hard X-ray microscopy [39,40]. This technique, however, has not yet been combined with XAS, so far.

A lot of information can be obtained from such a projection, as shown in Section 5. However, if the sample is inhomogeneous along the beam, the interpretation of single transmission images may not be sufficient for a reasonable characterization. In that case, tomographic imaging techniques are required. For tomographic imaging, a series of transmission images (projections) is recorded for a large number of angles over 180° or 360°. From these data, the three-dimensional inner structure of the sample can be reconstructed, yielding the attenuation coefficient $\mu(x, y, E)$ at each location inside the sample. By fitting normalized reference spectra to these data, the contribution of each chemical species to this attenuation can be extracted. Thus, the mass density of each component at each location on the virtual section can be determined quantitatively. The error in mass density can be estimated by the residual of the fit, provided no systematic errors have been made in identifying the right reference species used in the fit. We apply tomographic full-field imaging to shell-impregnated catalysts in Section 3. In general, it is time consuming to record full spectroscopic data (>6 h at present) in a tomographic scan even if a single full tomogram requires but a few minutes of acquisition time and typically data for only a few characteristic X-ray energies can be recorded. Recording full XANES tomograms also results in large datasets requiring new storage and computing infrastructure as well as optimized software (cf. Section 9).

3. X-ray tomography on shell-impregnated solid catalysts using an X-ray camera

The setup sketched in Fig. 1(b) was used to investigate the impregnation process of alumina pellets. Fig. 2 shows the tomographic image of a 0.5 wt% Pd/Al_2O_3 pellet with cylindrical shape (3.2 mm × 3.6 mm, Engelhard), which was recorded at beamline BW2 at HASYLAB. The photon energy was set to 18 keV and a pixel size of the camera of 2.3 μm was used (resulting in a spatial resolution of about 4 μm). The sample was rotated using a setup described in more detail in Refs. [41,42]. The results (Fig. 2) show that the microstructure of the grainy alumina pellet is visible. With a brighter contrast towards the pellet surface the impregnated part with the palladium constituent can be observed. The sharp gradient demonstrates that the front during impregnation has been very sharp, indicating a diffusion-controlled immobilization process. This is in line with electron microscopy studies (not shown), which however can only give

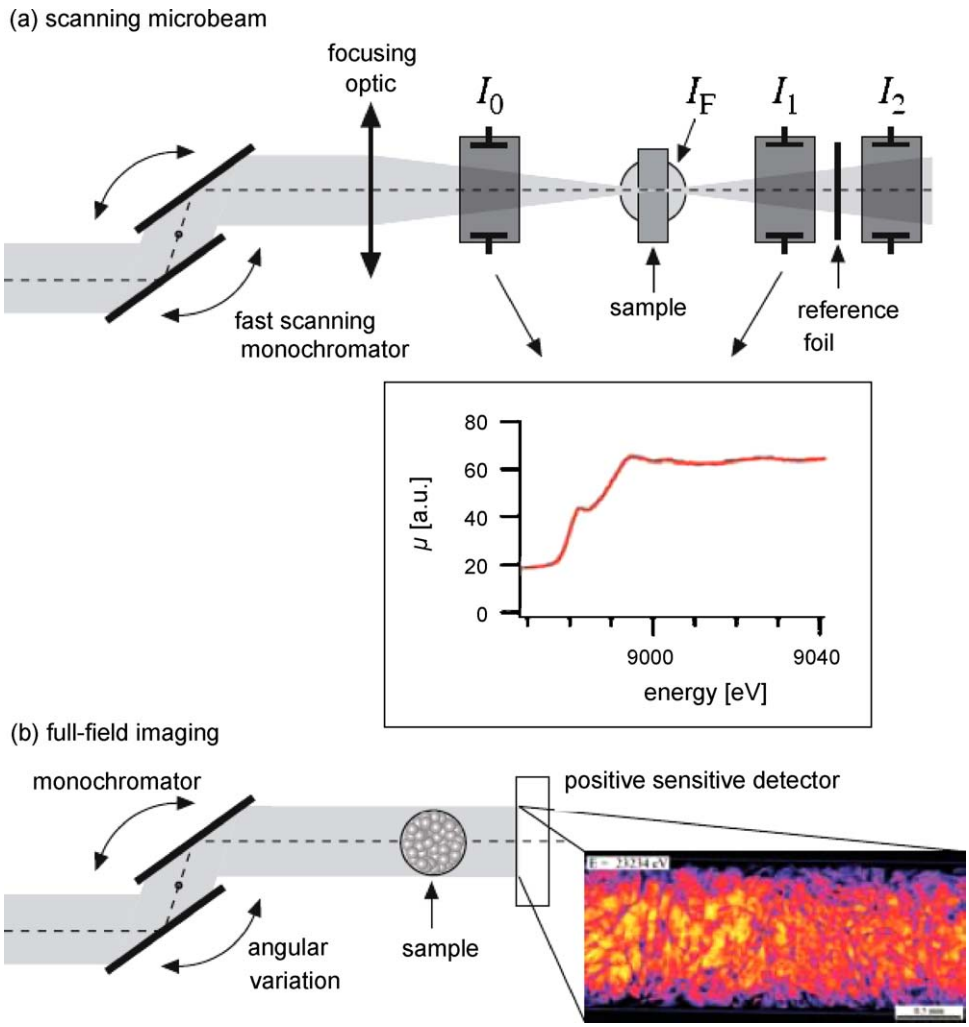

Fig. 1. Side views of the setups for spatially resolved X-ray absorption spectroscopy: (a) scanning microbeam with a focussing optics, a fast scanning monochromator and a sample stage with rotation and translation, allowing for tomographic data acquisition; detection in transmission by ionization chambers (I_0 and I_1) and/or in fluorescence by corresponding detectors (I_0 and I_F); (b) full-field imaging using a position sensitive detector and a conventional step scanning monochromator.

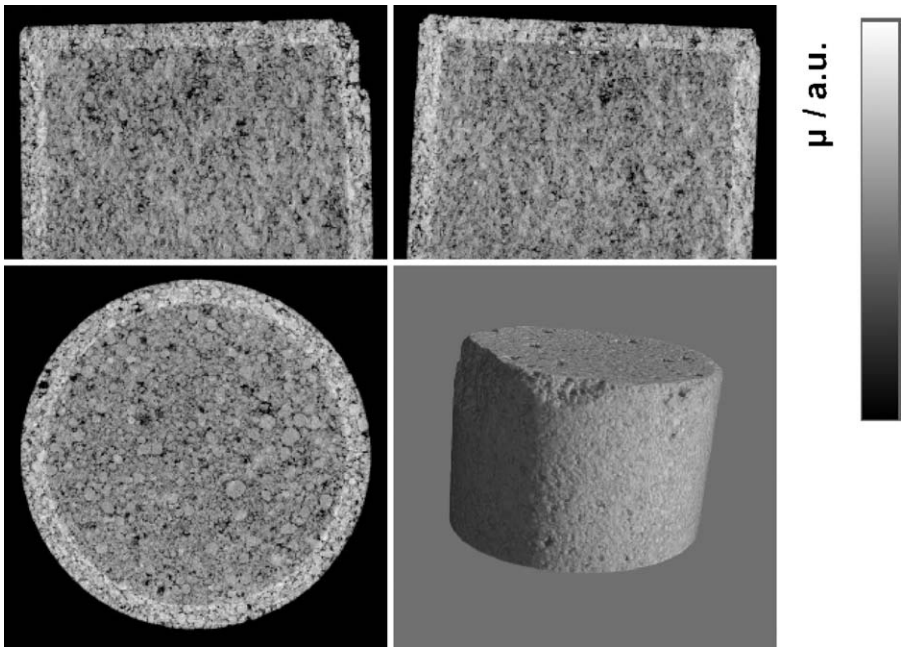

Fig. 2. 3D-reconstruction of a 0.5%Pd/Al_2O_3 catalyst pellet prepared by shell-impregnation; field of view: 3.54 mm × 2.36 mm; total reconstructed volume of 3.54 mm × 3.54 mm × 2.36 mm.

two-dimensional information whereas the data presented in Fig. 2 contains the information in three dimensions.

In the same manner Cu/Al_2O_3 catalysts, prepared by impregnation with $CuCl_2$-solution (according to Ref. [43]) and using alumina pellets of the same shape and size, were investigated. The results are depicted in Fig. 3(a) and (b). While the first catalyst was immersed for 1 min, the second one was kept in the impregnation solution for 10 min. The sharp diffusion front moved towards the centre of the pellet, which indicates a shell-progressive behaviour. Interestingly, certain differences can be found in the thickness of the impregnated part for the radial and axial direction (particularly in Fig. 3(a)), indicating some structural anisotropy, which was probably caused by the extrusion process used in the pellet manufacturing and results in different diffusion behaviours in the two directions. These results allow determining the progress and shape of the impregnation zone without cutting/destruction of the pellets. This strategy can be regarded complementary to micro-Raman, IR-, UV–vis, and magnetic resonance imaging techniques recently reported by Weckhuysen et al. [13,14] and is well suited for deriving a mathematical description of diffusion-controlled immobilization processes [44]. The use of this technique will also be of further relevance to identify the element distribution (in combination with fluorescence detection) and thus the microscopic structure of heterogeneous catalysts.

The same kind of information can be obtained for a quartz capillary microreactor by using a micro-focussed beam (5 μm × 5 μm), which is illustrated in Fig. 4. The interface between a catalyst bed composed of 5 wt%Pt/Al_2O_3 and the adjoining inert material (on the right side) was scanned stepwise. The experiment was performed at the Swiss Light Source (microXAS, SLS, Villigen) by using micro-focussing by a Kirkpatrick–Baez total reflection mirror system (KB-mirror) and a microbeam setup as in Fig. 1(a) with a step-scanning monochromator. First the X-ray absorption was measured in transmission at 11 578 eV (above the Pt L_3-edge) and then the experiment was repeated at 11 450 eV. By subtracting the X-ray absorption images at both energies, the strong X-ray absorption of the Pt-component could be extracted as shown in the image at the bottom. Since the X-ray attenuation coefficient $\mu(x, y)$ is directly related to the concentration of the element, 2D- and even 3D-concentration profiles can be derived. The same information can be derived by using X-ray fluorescence mapping (e.g. [45]). In both cases, however, the mapping is more time consuming than full-field microscopy but has the inherent advantage that selected points can be studied in more detail by micro-XAS or micro-XRD.

4. Analysing the oxidation state of copper in a catalyst bed using a micro-focussed X-ray beam (*ex situ* study)

In order to obtain full 3D structural information from the inside of a reactor capillary, we have combined X-ray absorption near-edge structure (XANES) spectroscopy with scanning microtomography. The experiment was performed at the Advanced Photon Source (Undulator Beamline 1-ID, Argonne National Laboratory, Chicago). The experimental setup corresponds to the one shown in Fig. 1(a). The synchrotron radiation beam was monochromatized by a fast scanning monochromator [46,47] that was synchronized with a fast data acquisition system, which reads the data from three ionization chambers and a PIN-diode, which assigns them to the corresponding energy. In this way, it was possible to record 10 full near edge spectra per second (8960–9040 eV) in a continuous operation. The monochromatized X-ray beam was then focussed onto the sample by refractive Be X-ray lenses to about 10 μm [48]. The incident and transmitted radiation was measured by two ionization chambers I_0 and I_1. At the same time, the transmission through a reference sample, i.e. a metallic foil of the element of interest, was measured using the signal from the ionization chambers I_1 and I_2. The fluorescence signal from the sample was measured simultaneously by a PIN-diode that faces the sample at 90° angle to the incident beam [cf. Fig. 1(a)].

In order to obtain local information from a virtual slice of the sample, XAS spectra have to be acquired at different translational and rotational positions. To record a single tomographic projection the sample is scanned in translation perpendicular to the beam. At each translational position, a full absorption spectrum is recorded. After the translational scan has been completed, the sample is rotated by an integer fraction of 360° and the next translational scan is performed. This procedure is repeated until the sample has completed a full rotation. For each energy of the absorption spectrum, the attenuation coefficient μ on a virtual section

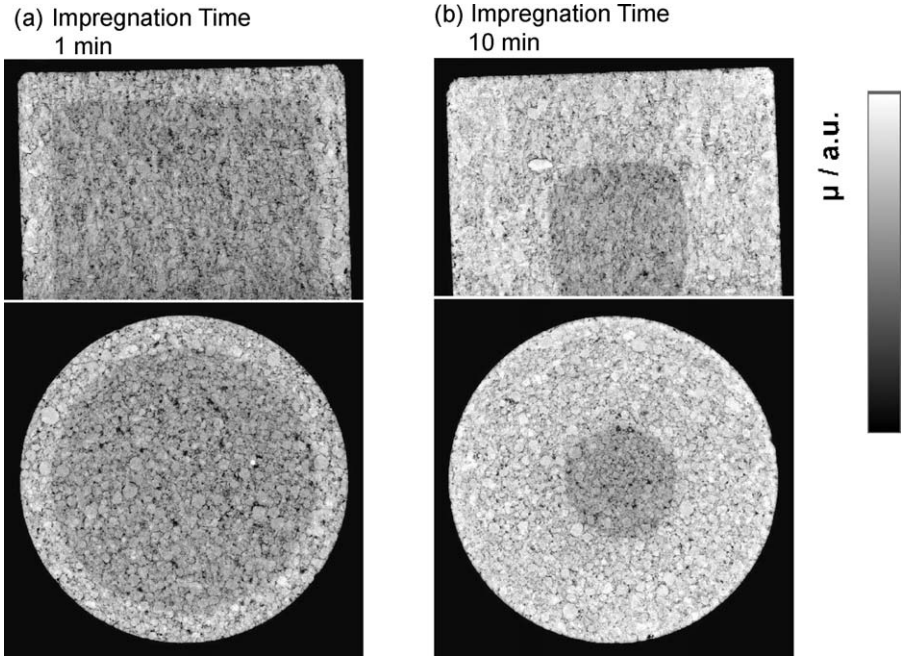

Fig. 3. 3D-reconstruction of Cu/Al_2O_3, (a) 1 min and (b) 10 min with $CuCl_2$-solution impregnated catalyst pellet; field of view: 3.54 mm × 2.36 mm.

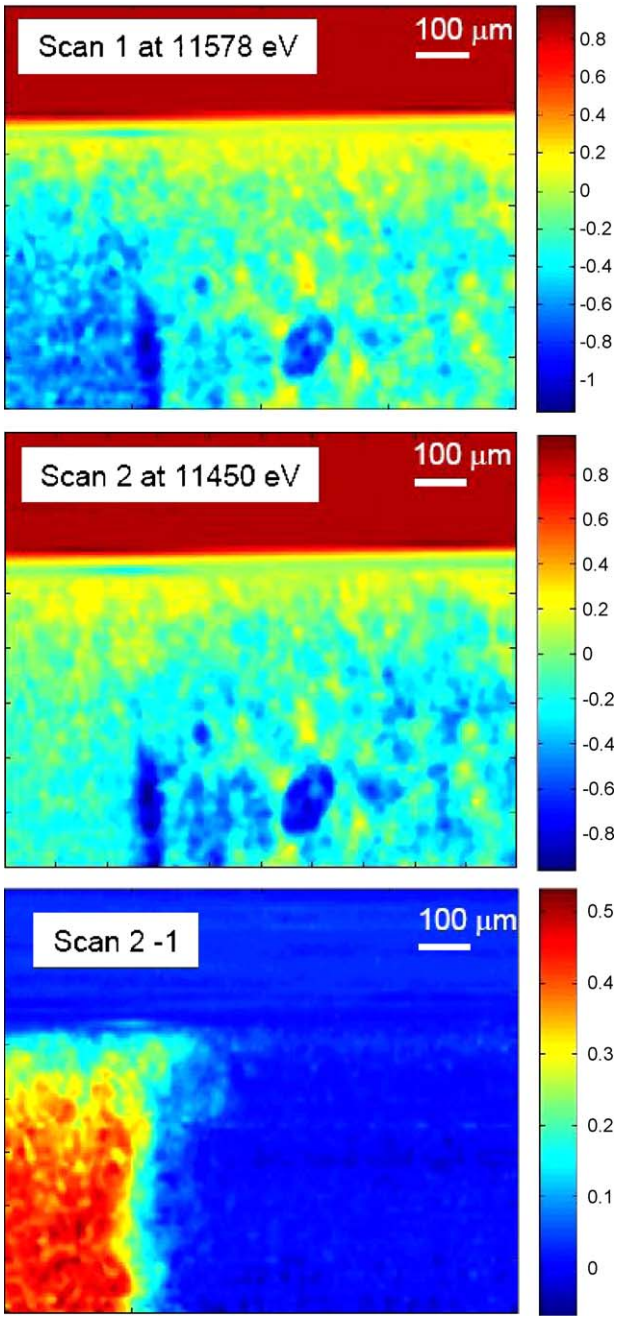

Fig. 4. 2D-maps of a catalytic reactor with catalyst bed (composed of 5 wt%Pt/Al_2O_3 and the adjoining inert material on the right) using a micro-focussed X-ray beam and two selected energies of 11 578 and 11 450 eV. The difference of the two scans shows the distribution of Pt inside the catalytic reactor.

through the sample is reconstructed tomographically, yielding a full absorption spectrum at each location inside the object. Note that the mass density of each component at each location on the virtual section could be determined quantitatively, as described in Section 2.

We have performed such a XANES-tomographic scan on a Cu/ZnO catalyst inside a glass capillary of about 500 μm in diameter at the Cu K-edge (cf. Ref. [35]). The scan consisted of 101 projections, each comprising 90 translational steps of 10 μm step size. In order to record the spectra in a reasonable time span, a QEXAFS monochromator was used (10 Hz, 10 000 points/spectrum, 10 scans per sampling position), which resulted in 90 000 spectra per virtual slice as depicted in Fig. 5. The figure also shows a schematic sketch of the sample and a reconstructed attenuation through the sample at an energy of 8 995 eV. In each point, however, the full spectrum of the corresponding Cu-component can be extracted, as shown for two points in Fig. 5(top). The comparison to Cu(II), Cu(I), and Cu(0) reference compounds reveals the concentration of the three components as well as that of the featureless background quantitatively (given as relative concentration in Fig. 5) and uncovers that most of the catalyst sample, which had been treated in cycles of 4%H_2/He and 2%O_2/He at 300 °C, was in a reduced state either of Cu(0) or Cu(I) and that hardly any Cu(II) was present. Fig. 5(bottom) shows the relative (percentage) distributions of metallic, mono-, and bivalent Cu as well as the attenuation due to other elements.

Since the combination of X-ray microscopy with absorption spectroscopy results in large data sets, they need to be evaluated in an automated fashion. Therefore, a special software was developed to automatically extract and calibrate all these spectra and reconstruct the tomographic data for each energy in the spectral range. After reconstruction, the absorption spectrum at each location in the reconstruction is available and can be fitted automatically to reference spectra. The analysis can be performed on state-of-the-art computers including laptops. To make this technique available to the non-expert users, a user-friendly interface is planned to be developed. In this way, the method could be used on a routine basis at microprobe beamlines at third generation synchrotron radiation sources.

5. Towards *in situ* studies: monitoring of the catalyst bed under reaction conditions using mapping with an X-ray beam

Concentration and temperature gradients can occur in a number of reactions. Therefore, it is important to combine integral *in situ* monitoring of the catalysts with local spectroscopic techniques. Obviously, such changes can occur in partial oxidation reactions because the concentration (and temperature) may change drastically over the catalysts bed, e.g. in the oxidation of methanol to formaldehyde [49], dehydrogenation of propane [50], oxidation of butane to maleic anhydride [51], propane to acrylonitrile [12] and the partial oxidation of hydrocarbons to synthesis gas [19,21,52,53]. In the latter reaction total oxidation/reforming and direct partial oxidation models have been proposed [53,54], which renders it an excellent model case. The knowledge of such gradients is important in order to optimize reactors (e.g. by modelling) and optimize heat and mass transfer in industrial applications.

In order to identify possible gradients, we studied the structural changes within the catalyst bed in a first step with a 0.5 mm × 1 mm large X-ray beam [18]. The experiments were performed at beamline X1 at HASYLAB (DESY, Hamburg, Germany). For the partial oxidation of methane on 2.5 wt%Rh–2.5 wt%Pt/Al_2O_3 oxidized platinum and rhodium species were found in the entrance zone of the catalyst bed and more reduced noble metal species towards the bed end [18]. In a more recent study, we then applied a 5 μm micro-focussed beam at the Swiss Light Source on a 5 wt%Rh–5 wt%Pt/Al_2O_3 (focussed with KB-mirror, cf. description for Fig. 4) to monitor the changes over the catalyst bed. For this purpose, XANES spectra were taken at the Pt L_3-edge at a chosen axial line in the middle of the catalyst bed with a step size of 5 μm; they are depicted in Fig. 6. The gradient occurs within less than 200 μm in a rather sharp manner (25 spectra are shown in Fig. 6(a)). Since recording full XANES spectra at each position of a two-dimensional scan with a step-scanning monochromator (instead of a QEXAFS monochromator) is too time consuming (>12 h), two-dimensional transmission images at selected X-ray energies were recorded. The approach is similar to the one in Fig. 4 taking here the 3 characteristic points

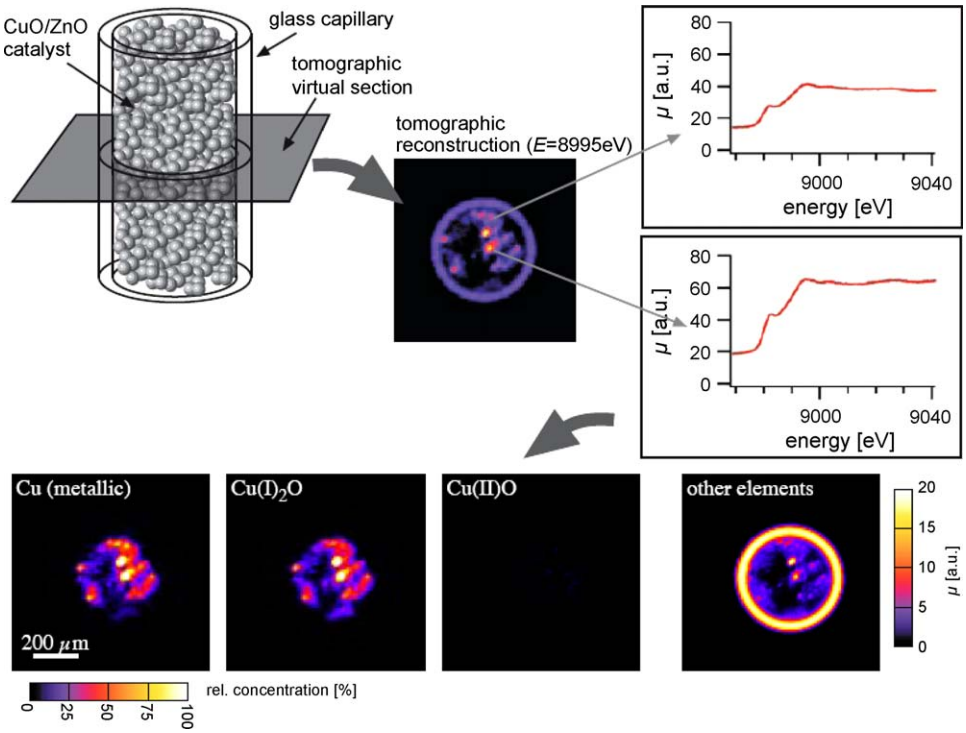

Fig. 5. Scanning microtomography combined with X-ray absorption spectroscopy at the Cu K-edge. In a virtual slice of a capillary (here catalyst bed containing Cu/ZnO-particles in BN) the X-ray absorption of the sample as function of energy is measured by scanning the sample in translation (90 steps of 10 μm each) and rotation (101 steps over 360°), acquiring at each position a full absorption spectrum (see also Fig. 1(a)); the absorption coefficient can be reconstructed for each energy at each location on the virtual slice. Thus, in each location on the reconstructed slice a full XANES (or EXAFS) spectrum is obtained. From these data the concentration of the different Cu-species can be extracted by fitting a linear combination of reference spectra to the spectrum at each location on the virtual slice.

at 11 555, 11 572 and 11 590 eV. Obviously, the X-ray absorption on the left side of the map (inlet side) is significantly larger than on the right-hand side. Note that only Pt L_3-data are shown here. Rh K-and Pt L_3-edge data (XANES and EXAFS) obtained with a ca. 100 μm large X-ray beam at selected points in the reduced and the oxidized part of the catalyst bed corroborate the conclusion that the noble metal species are in oxidized form at the beginning of the catalyst bed, whereas they are reduced at its end (not shown).

The different examples demonstrate that by using a micro-focussed beam, information on the structure within the catalyst bed can be obtained on the micrometer scale. Instead of the QEXAFS technique also dispersive EXAFS can be applied [8,55]. The utilization of micro-focussed beams can further help in deriving defined structural information at selected points. For low concentrated samples the same information can be obtained using fluorescence detection (see Fig. 1(a)). However, the scanning times required to obtain full two-dimensional maps can be very long and for 2D-XAS maps a sufficiently homogeneous sample density is required. For the acquisition of the image in Fig. 6, for example, 7.5 h were required, since a mapping at one of the characteristic energies took about 2.5 h.

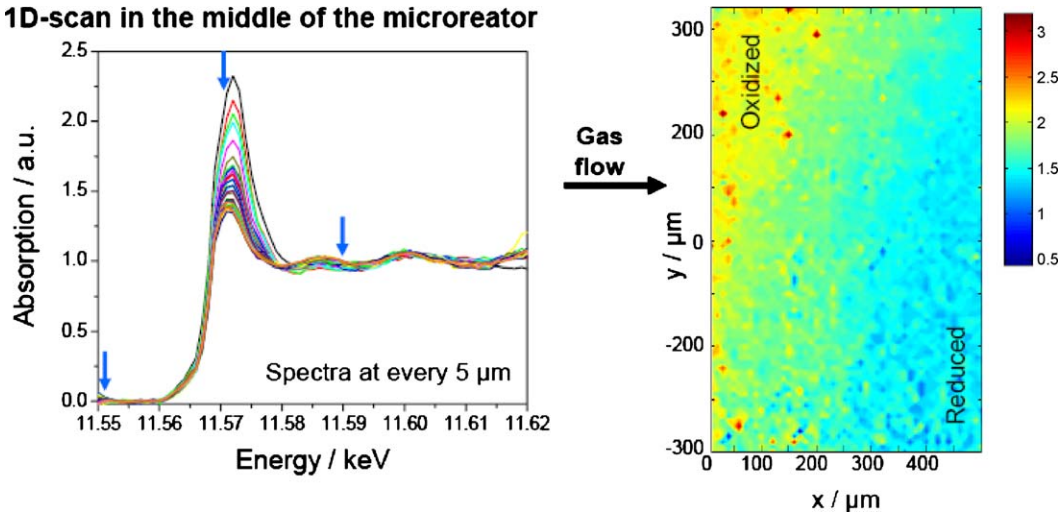

Fig. 6. *In situ* spectroscopic studies during the catalytic partial oxidation of methane in a quartz microreactor: axial profile of the Pt L_3-XANES of 5 wt%Pt–5 wt%Rh/Al_2O_3 in the middle of the reactor (left side) and the change in X-ray absorption that is a measure of the distribution of oxidized and reduced Pt-species (right side) by using a map of three indicated characteristic energy points (11.555, 11.572, 11.590 keV).

6. Spatially resolved XAS spectra using an X-ray camera

In order to speed up the acquisition time of the spectra one can also use full-field projection imaging with an X-ray camera as discussed in Fig. 1(b). Compared to a scan with a micro-focussed beam, where the sample has to be scanned in two dimensions, only the energy has to be changed and the intensities $I_0(x, y)$ and $I_1(x, y)$ are recorded by the camera. As the sample needs to be removed for flat-field images at each energy (cf. Section 2), a reproducible translation of the sample within the pixel size of the detector or a reproducible movement of the monochromator is required. The first case applies if the sample is moved in and out for each energy step, the latter if complete energy scans with and without sample are recorded after each other. In previous studies [19,56] we have demonstrated this principle and extracted such gradients (accuracy of the relative concentration of about 5%). The typical procedure is illustrated in Fig. 1(b) and was applied to a 2.5 wt%Pt–2.5 wt%Rh/Al_2O_3 catalyst during the partial oxidation of methane, operated in a similar manner as in Fig. 6. The experiment was performed at beamline X1 at HASYLAB using a high-resolution X-ray camera [19,56]. The catalytic performance was determined simultaneously with on-line mass spectrometry. Up to 150 X-ray absorption images as function of energy were recorded by acquiring images with and without the sample. Some typical flat- and dark-field corrected transmission images around the Pt L_3-edge (left side) and the Rh K-edge (right side) are shown in Fig. 7. Above the respective absorption edge the X-ray absorption significantly increases in both cases. Considering that the 150 images cover a view of the capillary of 3 mm × 1.5 mm and a resolution of about 10 μm, about 45 000 spectra can be extracted. This demonstrates the advantage of the present full-field over the scanning technique, in particular with acquisition times for single images in the 0.5 s range at third generation synchrotron radiation sources. There, the whole acquisition would take less than 5 min for XANES. Note that due to the improvement of computer power and availability of large data storage capacities, the analysis can be performed on state-of-the-art computational equipment (stationary and mobile systems).

The results from a linear combination of the XAS data extracted from the 150 images both at the Pt L_3- and the Rh K-edge during partial oxidation of methane at 322 °C are depicted in Fig. 8. Obviously, for both elements a sharp gradient is found. Here, two species were assumed which is in accordance with EXAFS analysis at the beginning and the end of the reactor and concentration profiles can be extracted quantitatively as demonstrated in Ref. [19]. The featureless background is similar at both absorption edges. Note that a small difference in the length of the zone of oxidized noble metals is found which is due to the fact that the reaction slowly extinguishes with time under the chosen reaction parameters and the measurement of the gradient at both edges was recorded sequentially, each taking about 1.5 h. This has recently been studied in more detail [57]. The comparison of the results at the Pt L_3- and Rh K-edge with their different X-ray absorption features around the edge and the different energy show that the strategy of using a camera is generally applicable provided the sample shows sufficient transmission and enough contrast in the characteristic features of the XANES spectra for the different structures inside the sample.

7. Spatiotemporal changes: extending time-resolved studies from integral to spatially resolved studies

Spatiotemporal changes on catalytic surfaces have spurred the community latest since the investigation of chemical oscillations that can be visualised for instance by using surface science techniques [58,59]. Dynamic changes can also occur on a micrometer scale, e.g. during ignition and extinction of a catalytic reaction [16,60]. For this purpose the catalytic partial oxidation of methane on noble metals (2.5 wt%Rh–2.5 wt%Pt/Al_2O_3 as mentioned above) is an excellent example: DRIFTS studies and QEXAFS measurements both at the Pt L_3- and Rh K-edge show that the noble metal components are reduced within a few seconds. In addition, on-line mass spectroscopy demonstrates that the product composition changes abruptly in a few seconds [61,62]. Considering the gradient during partial oxidation of methane (Figs. 6 and 8) equivalent studies should be performed in the same manner using,

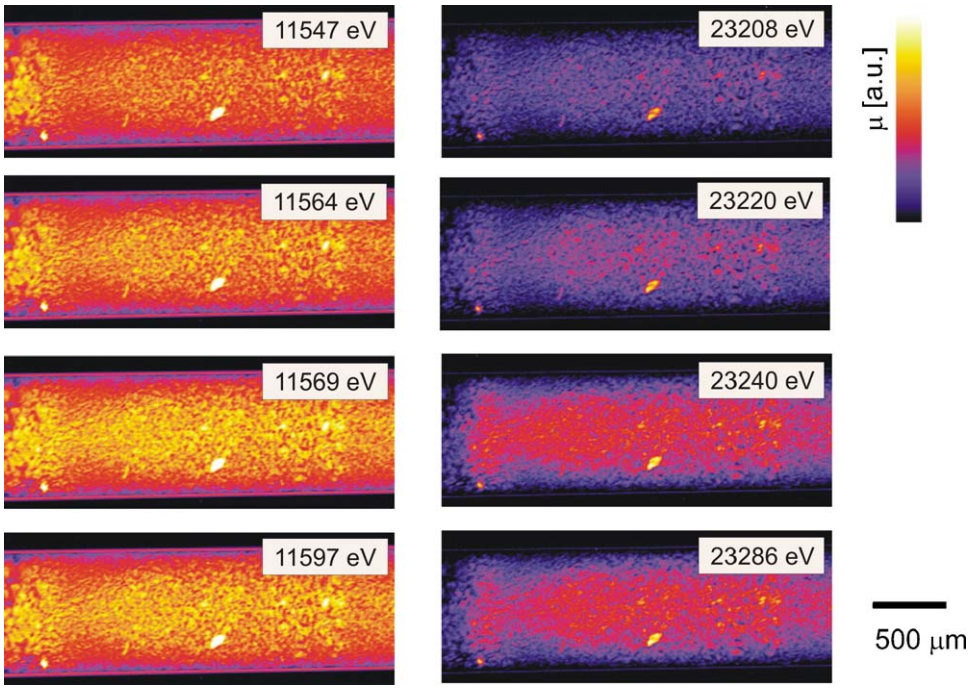

Fig. 7. Flat- and dark-field corrected transmission images of 2.5 wt%Pt–2.5 wt%Rh/Al_2O_3 inside the spectroscopic cell at different energies during the partial oxidation of methane at 283 °C: (left) around the Pt L_3-edge and (right) around the Rh K-edge.

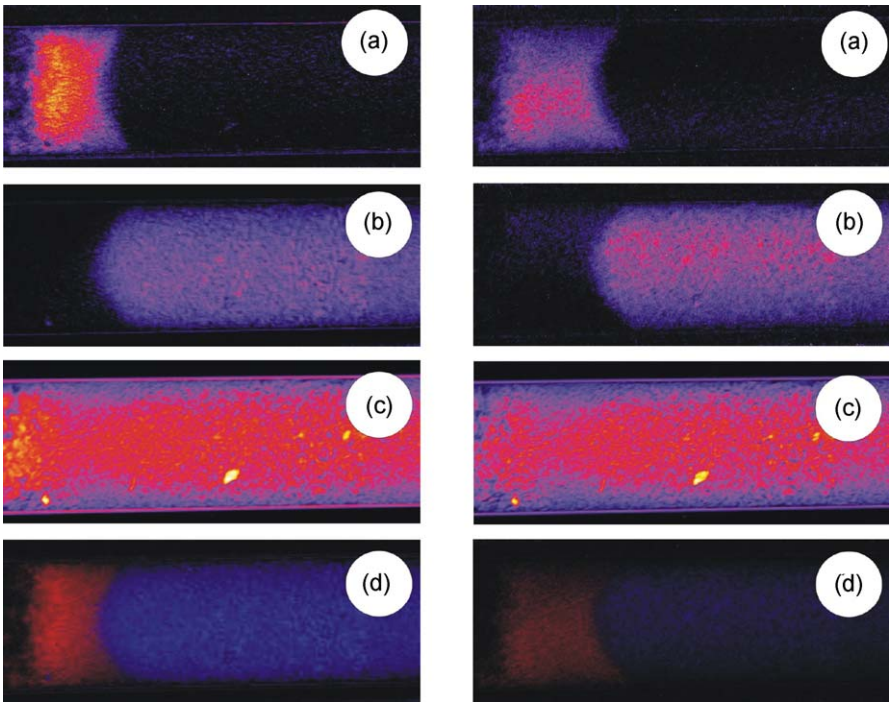

Fig. 8. Amount of oxidized (a) and reduced (b) noble metal species and their distribution for rhodium (left) and platinum (right) during the partial oxidation of methane at 322 °C over 2.5 wt%Pt–2.5 wt%Rh/Al_2O_3. (c) Featureless background with absorption that is not due to Rh K or Pt L_3 absorption; the brighter the colour, the higher is the relative concentration of the corresponding species. (d) Distributions of oxidized (red) and reduced (blue) Rh and Pt. (For interpretation of the references to colour in this figure legend, the reader is referred to the web version of the article.)

e.g. an X-ray camera. However, changes at the subsecond scale cannot be imaged by recording full spectra, as described in the previous section. Tuning the energy of the incoming X-rays to the maximum of the whiteline at the Pt L_3-edge (11 596 eV) and using a fast read-out camera, a decrease of absorption should be visible at those parts of the microreactor, where the platinum constituent is reduced. Hence, a so-called FReLoN (fast readout low noise) camera developed at ESRF [63,64] was placed behind the catalytic microreactor. The experiment was performed at beamline ID26 at ESRF to benefit from the high monochromatic photon flux (here ca. 5.2×10^{12} photons/s, beam size 1 mm^2) of a third generation synchrotron radiation source. By collecting X-ray transmission images of the catalytic microreactor with a frame rate of 1 s^{-1} (200 ms exposure time per image), a strong structural change of the catalyst was observed when the ignition of the reaction from methane and oxygen to hydrogen and carbon monoxide started. Fig. 9 shows a sketch of the experimental setup, a transmission image through the reactor, and a series of images recorded at different times during the ignition of the reaction. The latter were obtained by subtraction of the X-ray absorption images at different times t from those recorded before the ignition temperature (such as in the first image) to emphasize the difference in absorption and to correct for inhomogeneities in the sample. A full series of pictures corresponding to the ignition in Fig. 9 is assembled in the movie enclosed in the electronic support information. It shows the propagation of the frontier between oxidized and reduced Pt species starting at the outlet and moving towards the inlet of the reactor. The observed reduction of the noble metal occurred at the same time as the ignition of the chemical reaction (detected by on-line gas analysis using a mass spectrometer), as several ignition/extinction cycles showed, where the camera was placed at the end of the catalyst bed. Note that heat was provided from the bottom, which results – on the μm-scale – in an asymmetric profile.

The movie and the selected images in Fig. 9 also show that in the beginning of the sequence the front is rapidly moving through the reactor, whereas it slows down in the end. This is due to the fact that the position of the camera was carefully chosen to be able to monitor the stabilization of the gradient at its stationary position (e.g. corresponding to the stationary gradient in Fig. 8).

In related experiments on the same reaction system temperature profiles were followed using an IR-thermography camera (ThermaCAM 63, Pergam Suisse AG) with close-up lens and a typical recording time of about 1 frame per second. Some of the observed axial changes are depicted in Fig. 10. Obviously, the exothermic reaction (total oxidation of methane) leads to a self-heating of the catalyst. As soon as the partial oxidation of methane ignites an even more pronounced hot spot forms that moves towards the beginning of the catalyst bed—in the same manner as the front of reduction. Further heating to higher temperatures leads to a further movement towards the beginning of the catalyst bed, which is in agreement with the stationary experiments given in Section 5.

The movement of the front from the outlet towards the inlet can be explained with a total oxidation-reforming mechanism. At first, below the ignition temperature, methane is fully combusted to carbon dioxide and water over the whole length of the catalyst bed. At some moment, the temperature reaches the ignition point which leads to a self-heating of the catalyst bed and thus strong consumption of oxygen. As soon as some metallic species form (preferentially at the end of the reactor), they promote the activation of methane and thus lead to the formation of hydrogen and carbon monoxide. This again leads to an enhancement in the formation of hydrogen and carbon monoxide. The reduction propagates towards the inlet of the reactor, where the total oxidation of methane still occurs over oxidized noble metal particles (similar to the situation below the ignition temperature where the noble metal is mainly oxidized and the total oxidation of methane is observed). More recently, we extended these studies and found that the ignition starts at some catalyst particles of the sieve fraction of 100 μm and then continues through the catalyst bed towards the inlet [65].

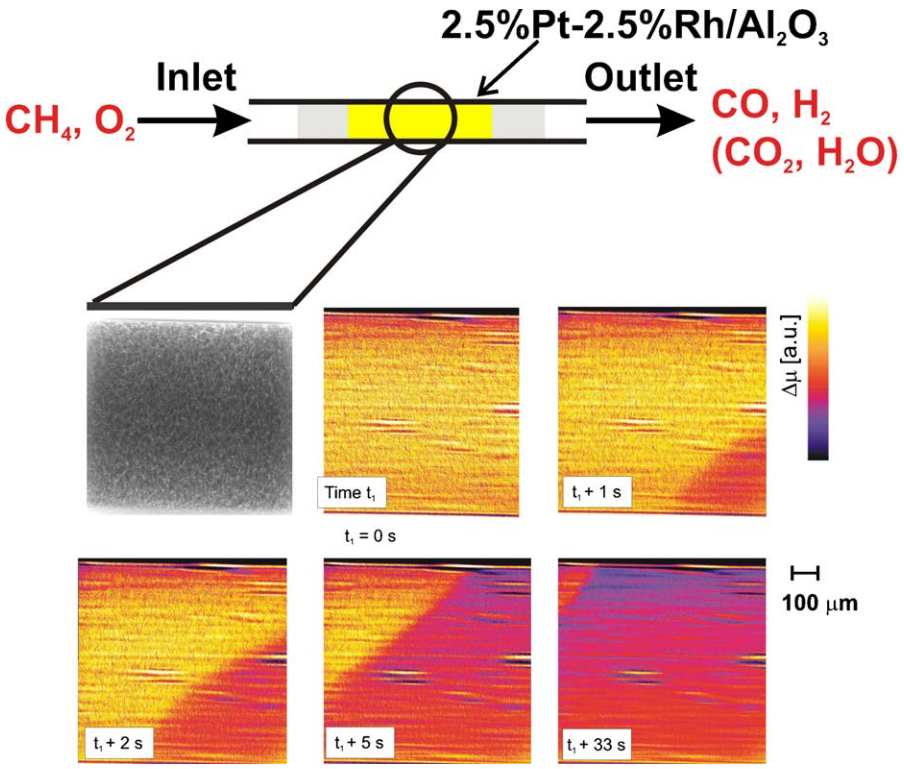

Fig. 9. Schematic sketch of the catalytic microreactor for partial oxidation of methane to carbon monoxide and hydrogen (CPO) on a 2.5%Pt–2.5%Rh/Al_2O_3 catalyst and snapshots during the ignition of the CPO reaction. A 1 mm × 1 mm snapshot taken with the FReLoN camera is depicted in gray colour and the X-ray absorption images recorded at the whiteline energy of Pt (Pt L_3-edge; 11 586 eV) as function in the time interval t_1 to t_1 + 33 s in colour (obtained by subtraction of the X-ray absorption image at time t and collected at $t < t_1$; t_1 is the time of the last image where no gradient was found in the images; dark red and blue colour indicate lower absorption of X-rays); the movie assembled from all the pictures is given as electronic support information; cf. Ref. [85]. (For interpretation of the references to colour in this figure legend, the reader is referred to the web version of the article.)

This example demonstrates that it is essential to determine the structure of a catalyst not only *in situ* but also in a spatiotemporally resolved manner. Thereby, important insight into the mechanism of the catalytic reaction can be gained. In particular, it allows understanding of start-up phases of catalytic reactors including activation and reaction mechanisms in more detail. Also reactor instabilities as occurring in chemical oscillations may be studied in future [66].

8. Further application of spatially and time-resolved X-ray absorption spectroscopy

The applicability of micro-focussed X-rays in spatially resolved studies goes beyond the examples presented here. It is well known that micro-focussed X-ray beams can be used for understanding a wide variety of heterogeneous samples [34–36,67–69]. But also in related applications, for example for investigating microreactors or other devices structured on a micro- to millimeter scale, the use of a micro-X-ray beam may be used advantageously. A related subject, employing mm-large beams, is robot-controlled sample handling in combination with small beams for high throughput characterization of heterogeneous catalysts [70]. This can be efficiently done on special and small reactor devices.

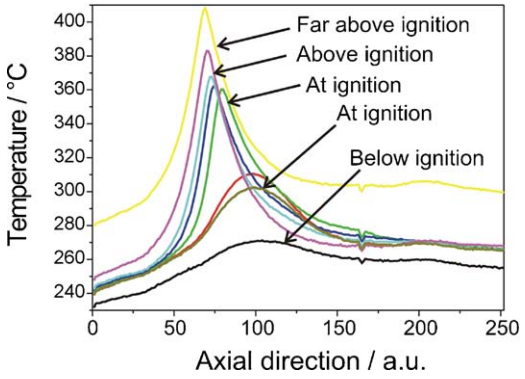

Fig. 10. Development of the temperature gradient during the ignition of the catalytic partial oxidation of methane; recorded with an infrared camera; recorded below ignition, at the ignition temperature and above the ignition temperature.

The same applications as for micro-focussed beams are – as presented in Section 5 – also possible by using an X-ray camera. Also in this case reactors structured in the mm or cm-length scale can be investigated. To show this principle, we applied the technique for parallel screening of heterogeneous catalysts. Such a special cell for the "proof of concept" is depicted in Fig. 11. The cell is composed of 10 compartments in this case filled with Pd-catalysts (for details, cf. Ref. [71]) and both a beam with 0.5 mm × 0.5 mm as well as full-field microscopy were employed at beamline X1 at HASYLAB. The use of the X-ray camera allows recording the spectra in each compartment in a parallel manner and thus under dynamic reaction conditions; the spectra are recorded in a real simultaneous way. This is for example advantageous for temperature-programmed reduction/reaction experiments. During data acquisition for the high throughput parallel characterization of catalysts a stack of transmission images of the whole microreactor array is recorded as a function of X-ray energy. From these data, the absorption spectra for the different catalysts are extracted by integrating the transmission through each of the microreactors in the array over all the pixels behind it. In the current study, this was done by manually masking the relevant areas in the transmission images. As the whole data acquisition procedure can be standardized, these areas in the

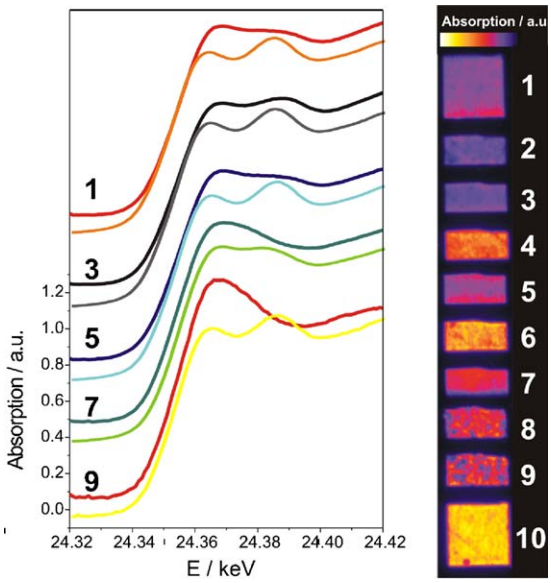

Fig. 11. X-ray transmission image of a microreactor array (right, tilted by 90°) filled with ten different palladium catalysts; selected spectra before and after reduction (top and bottom spectrum, respectively) of five selected catalyst samples: (1) 5 wt% Pd/Al_2O_3, Engelhard 40692 (pre-reduced in commercial process, stored in air); (3) 5 wt% Pd/Al_2O_3, Engelhard 40692, freshly pre-reduced in hydrogen at 100 °C and then exposed to air; (5) 5 wt% Pd/Al_2O_3, Engelhard 40692 (pre-reduced in commercial process, stored in air); (7) flame spray pyrolysis, using methanol/acetic acid mixtures according to Ref. [86]; (9) $Pd_{33}Zr_{67}$ alloy oxidized in air according to Refs. [87,88].

transmission image are determined once and fed into an automatic procedure to extract the spectra in the different microreactors. This method can therefore be made available on a routine basis, preferably using a user-friendly interface.

Fig. 11 shows the extracted XANES spectra of five selected Pd catalysts that were recorded after preparation and after *in situ* reduction at room temperature. Significant changes are observed, also during re-oxidation in air (cf. Ref. [71]). The same principle could recently be used to record the structure of six catalysts at the same time under reaction conditions uncovering significantly different structure of the catalysts under reaction conditions which is related to their catalytic activity [72] and can be compared to infrared spectroscopic studies with focal plane array detectors to perform chemical product analysis or the determination of the temperature (IR-thermography) in high throughput reactor systems [73–75].

9. Outlook and conclusions

The examples presented in this overview demonstrate that time-resolved and spatially resolved spectroscopic studies are important for understanding the preparation of catalysts, the structural changes under dynamic conditions (e.g. activation of catalysts and start-up) and the structure of catalysts under reaction conditions. One important example of the beneficial application of spatially resolved spectroscopy in catalyst preparation is the impregnation of pre-shaped catalyst support materials such as extrudates. The ignition and extinction of reactions is a prominent example of studies under dynamic change of the reaction conditions. Finally, under stationary reaction conditions, variation of the catalyst structure along the catalyst bed or a catalyst pellet/particle can occur if gradients in reactant/product composition or temperature are present.

Among the different spectroscopic techniques, XAS and related techniques appear attractive, particularly to identify such variations on a micrometer scale and under real reaction conditions. They are complementary to other *in situ* spectroscopic techniques such as micro-infrared and Raman spectroscopy, which probe the vibrational bands, and electron microscopy that probes on an atomic scale and only recently allowed studies towards real reaction conditions [25]. In addition, the penetration depth of X-rays is advantageous, which allows constructing devices that mimic real systems. However, this requires a lot of effort in building up the catalytic experiments at the synchrotron radiation source, but at sources like HASYLAB in Hamburg, SLS in Villigen, ESRF in Grenoble, and NSLS in Brookhaven an environment has been recently established that is ideal for *in situ* studies and more equipment for catalytic studies is or will be directly available in the near future. There is a general trend of the synchrotron radiation facilities to combine various techniques at the same time (e.g. Raman spectroscopy, infrared spectroscopy, XRD, etc.) and to provide them to the user which greatly enhances the development in this rapidly growing field and encourages catalysis researchers to apply these techniques that have previously been reserved for specialists. Finally, equipment for time-resolved studies dedicated to catalysis are permanently installed at several synchrotron radiation beamlines. The same trend will hopefully come up soon in spatially resolved studies, which will make these investigations more amenable in the future and allows their extension to various other catalytic systems. Note that larger amounts of data are collected in spatially resolved studies than in standard integral spectroscopic studies, but the analysis is, with current IT-equipment, not a problem any more and, as outlined in previous sections, user-friendly versions of the codes will be available in the future. In a next step, full-field X-ray absorption spectroscopic tomography is desirable. This will require significant investments in the storage and computing infrastructure as well as in optimized software, since a volume section instead of a slice and a full XANES spectrum instead of characteristic points are recorded and raw data in the range of 1 TB per tomogram needs to be stored and processed.

For spatially resolved X-ray absorption spectroscopic studies and tomographic investigations with XAS, different approaches using full-field and scanning microscopy can be applied. The use of full-field microscopy with an X-ray camera gives the possibility of parallelization, a microbeam can only be efficiently used for determining the different structure by XAS using the QEXAFS or DEXAFS technique. In both cases not only the X-ray contrast but also the structure can be derived. Compared to full-field imaging, scanning microscopy is significantly slower, as the sample is scanned point by point. However, it can be applied to dilute systems using the fluorescence signal for absorption spectroscopy and, since achromatic optics can be used in scanning microscopy, it is much easier to extend the absorption spectrum to the full EXAFS regime than in the case of full-field microscopy. The latter has, however, so far not been demonstrated experimentally.

The spatial resolution is either limited by the resolution of the camera (typically 1 μm) or the size of the microbeam. To improve the spatial resolution in full-field imaging, magnified imaging is needed [76]. Currently, spatial resolutions in the 100 nm range can be achieved with hard X-rays. Hard X-rays can be focussed down to well below 100 nm [77–80] and it is expected that in the near future even resolutions down to 10 nm can be achieved in scanning microscopy [81,82]. In addition, coherent X-ray diffraction imaging (CXDI) can be combined with absorption spectroscopy [83]. In combination with X-ray focusing, 5 nm spatial resolution was demonstrated for this technique [84] that can potentially be improved to the 1–2 nm scale. This will allow significantly better resolutions than illustrated in the present examples. In general, the use of the micro-focussed beam appears to have advantages at such small length scales but also if the structure should be identified in a selected area or in selected point. Another challenge

is *in situ* tomographic X-ray absorption spectroscopy under reaction conditions that will give even better insight, e.g. into gradients occurring in catalytic reactors. For this purpose, apart from a modified reaction cell, high intensity beamlines with a stable monochromator combined with an X-ray camera or highly focussed beams at third generation synchrotron sources will be needed and will give insight into the mechanism of catalytic reactions.

The spatiotemporal identification of structural changes in catalyst fixed-beds can be further achieved in the subsecond scale if significant differences in X-ray intensity upon change in oxidation state/geometry of the element of interest are observed. Such rapid changes occur not only in the case of ignition/extinction of catalytic reactions as demonstrated in the present example but also if the gas composition/reaction conditions are changed inside a reactor or if transient phenomena or oscillations occur. This is not limited to heterogeneously catalysed reactions but may also be applied to reactions/oscillations in solutions.

Finally, the application of the full-field microscopic technique for characterizing catalysts in a parallel manner shows that the technique can also be applied in a fully different topic: high throughput and parallel characterization of several catalysts under reaction conditions. This application may initiate also similar activities in related fields, e.g. in microreactor devices with several channels or other devices on a micrometer scale where different structures are of importance and expected on a microscale, or where global spectroscopic methods are not applicable. Note that these techniques may be beneficially combined with micro-IR, micro-XRF and XRD, micro-Raman and micro-UV–vis studies.

Acknowledgements

We thank HASYLAB at DESY (beamlines X1 and BW2, Hamburg, Germany), the APS (Chicago, USA), ESRF (ID26, Grenoble, France), and SLS (microXAS, Villigen, Switzerland) for granting beamtime for the different projects. In addition, financial support by ESRF, the European Community—Research Infrastructure Action under the FP6: "Structuring the European Research Area" ("Integrating Activity on Synchrotron and Free Electron Laser Science" (IA-SFS) RII3-CT-2004-506008), DANSCATT and Karl Winnacker grant (JDG) are acknowledged. Pergam Suisse AG (Zurich, Switzerland) is thanked for support and borrowing the infrared camera. Moreover, we thank R. Frahm, D. Lützenkirchen-Hecht (University Wuppertal), A. Webb, E. Welter (HASYLAB), J. Herzen, T. Donath (GKSS), D. Grolimund (SLS), and S. Hannemann, P. Trüssel, and R. Mäder (ETH Zurich) for their support.

Appendix A. Supplementary data

Supplementary data associated with this article can be found, in the online version, at doi:10.1016/j.cattod.2008.11.002.

References

[1] D.C. Koningsberger, R. Prins, X-ray Absorption: Principles, Applications, Techniques of EXAFS, SEXAFS, and XANES, Wiley, New York, 1988.
[2] Y. Iwasawa, X-ray Absorption Fine Structure for Catalysts and Surfaces, World Scientific, Singapore, 1996.
[3] B.S. Clausen, H. Topsøe, R. Frahm, Adv. Catal. 42 (1998) 315.
[4] G. Sankar, J.M. Thomas, Top. Catal. 8 (1999) 1.
[5] D. Bazin, J. Lynch, M. Ramos-Fernandez, Oil Gas Sci. Technol. 58 (2003) 667.
[6] G. Meitzner, S.R. Bare, D. Parker, H. Woo, D.A. Fischer, Rev. Sci. Instrum. 69 (1998) 2618.
[7] J.-D. Grunwaldt, B.S. Clausen, Top. Catal. 18 (2002) 37.
[8] M.A. Newton, A.J. Dent, J. Evans, Chem. Soc. Rev. 31 (2002) 83.
[9] J.-D. Grunwaldt, M. Caravati, S. Hannemann, A. Baiker, Phys. Chem. Chem. Phys. 6 (2004) 3037.
[10] J.-D. Grunwaldt, A. Baiker, Phys. Chem. Chem. Phys. 7 (2005) 3526.
[11] A. Brückner, Catal. Rev. Sci. Eng. 43 (2003) 97.
[12] M.A. Banares, Catal. Today 100 (2005) 71.
[13] A.A. Lysova, I.V. Koptyug, R.Z. Sagdeev, V.N. Parmon, J.A. Bergwerff, B.M. Weckhuysen, J. Am. Chem. Soc. 127 (2005) 11916–11917.
[14] L. Espinosa-Alonso, K. de Jong, B.M. Weckhuysen, J. Phys. Chem. C 112 (2008) 7201.
[15] F. Basile, G. Fornasari, F. Trifirò, A. Vaccari, Catal. Today 64 (2001) 21.
[16] R. Schwiedernoch, S. Tischer, C. Correa, O. Deutschmann, Chem. Eng. Sci. 58 (2003) 633.
[17] B. Li, K. Maruyama, M. Nurunnabi, K. Kunimori, K. Tomishige, Ind. Eng. Chem. Res. 44 (2005) 485.
[18] J.-D. Grunwaldt, A. Baiker, Catal. Lett. 99 (2005) 5.
[19] J.-D. Grunwaldt, S. Hannemann, C.G. Schroer, A. Baiker, J. Phys. Chem. B 110 (2006) 8674.
[20] J.-D. Grunwaldt, S. Hannemann, P. Boye, C.G. Schroer, A. Baiker, Highlight of analytical chemistry, Chimia 60 (2006) 709.
[21] R. Horn, N.J. Degenstein, K.A. Williams, L.D. Schmidt, Catal. Lett. 110 (2006) 169.
[22] R. Horn, K.A. Williams, N.J. Degenstein, A. Bitsch-Larsen, D.D. Nogare, S.A. Tupy, L.D. Schmidt, J. Catal. 249 (2007) 380.
[23] Y. Liu, F.-Y. Huang, J.-M. Li, W.-Z. Weng, C.-R. Luo, M.-L. Wang, W.-S. Xia, C.-J. Huang, H.-L. Wan, J. Catal. 256 (2008) 192.
[24] S. Helveg, C. Lopez-Cartes, J. Sehested, P.L. Hansen, B.S. Clausen, J.R. Rostrup-Nielsen, F. Abild-Pedersen, J.K. Nørskov, Nature 427 (2004) 426.
[25] S.B. Simonsen, S. Dahl, E. Johnson, S. Helveg, J. Catal. 255 (2008) 1.
[26] A.M. Beale, S.D.M. Jacques, J.A. Bergwerff, P. Barnes, B.M. Weckhuysen, Angew. Chem. Int. Ed. 46 (2007) 8832.
[27] L. Heinke, C. Chmelik, P. Kortunov, D.M. Ruthven, D.B. Shah, S. Vasenkov, J. Kaerger, Chem. Eng. Sci. Technol. 30 (2007) 995.
[28] E. Stavitski, M.H.F. Kox, I. Swart, F.M.F. de Groot, B.M. Weckhuysen, Angew. Chem. Int. Ed. 47 (2008) 3543.
[29] G. Mestl, C. Linsmeier, R. Gotschall, M. Dieterle, J. Find, D. Herein, J. Jäger, Y. Uchida, R. Schlögl, J. Mol. Catal. A 162 (2000) 455.
[30] J.A. Bergwerff, T. Visser, J.R.G. Leliveld, B.D. Rossenaar, K.P.d. Jong, B.M. Weckhuysen, J. Am. Chem. Soc. 126 (2004) 14548.
[31] J.A. Bergwerff, T. Visser, B.M. Weckhuysen, Catal. Today 130 (2008) 117.
[32] L.F. Gladden, Top. Catal. 24 (2003) 19.
[33] I.V. Koptyug, A.A. Lysova, R.Z. Sagdeev, V.A. Kirillov, A.V. Kulikov, V.N. Parmon, Catal. Today 105 (2005) 464–468.
[34] B. Lengeler, C. Schroer, J. Tümmler, B. Benner, M. Richwin, A. Snigirev, I. Snigireva, M. Drakopoulos, J. Synchrotron Radiat. 6 (1999) 1153.
[35] C.G. Schroer, M. Kuhlmann, T.F. Günzler, B. Lengeler, M. Richwin, B. Griesebock, D. Lützenkirchen-Hecht, R. Frahm, E. Ziegler, A. Mashayekhi, D.R. Haeffner, J.-D. Grunwaldt, A. Baiker, Appl. Phys. Lett. 82 (2003) 3360.
[36] P.M. Bertsch, D.B. Hunter, Chem. Rev. 101 (2001) 1809.
[37] C. Rau, A. Somogyi, A. Simionovici, Nucl. Instrum. Methods Phys. Res. B 203 (2003) 444.
[38] F. Beckmann, in: A.R.P.W. Reimers, A. Schreyer, H. Clemens, (Ed.), Neutrons and Synchrotron Radiation in Engineering Materials Science, Wiley-VCH, Weinheim, pp. 287–370.
[39] C.G. Schroer, J. Meyer, M. Kuhlmann, B. Benner, T.F. Günzler, B. Lengeler, C. Rau, T. Weitkamp, A. Snigirev, I. Snigireva, Appl. Phys. Lett. 81 (2002) 1527.
[40] Y.S. Chu, J.M. Yi, F.D. Carlo, Q. Shen, W.-K. Lee, H.J. Wu, C.L. Wang, J.Y. Wang, C.J. Liu, C.H. Wang, S.R. Wu, C.C. Chien, Y. Hwu, A. Tkachuk, W. Yun, M. Feser, K.S. Liang, C.S. Yang, J.H. Je, G. Margaritondo, Appl. Phys. Lett. 92 (2008) 103119.
[41] F. Beckmann, U. Bonse, T. Biermann, Proc. SPIE 3772 (1999) 179.
[42] F. Beckmann, T. Donath, J. Fischer, T. Dose, T. Lippmann, L. Lottermoser, R.V. Martins, A. Schreyer, Proc. SPIE 6318 (2006) 631810–631811.
[43] A. Baiker, W.L. Holstein, J. Catal. 84 (1983) 178.
[44] A.V. Neimark, L.I. Kheifez, V.B. Fenelow, Ind. Eng. Chem. Proc. Res. Dev. 20 (1981) 439.
[45] M. Vespa, R. Dähn, D. Grolimund, M. Harfouche, E. Wieland, A.M. Scheidegger, J. Geochem. Explor. 88 (2006) 77.
[46] J.-D. Grunwaldt, D. Lützenkirchen-Hecht, M. Richwin, S. Grundmann, B.S. Clausen, R. Frahm, J. Phys. Chem. B 105 (2001) 5161.
[47] M. Richwin, R. Zaeper, D. Lützenkirchen-Hecht, R. Frahm, J. Synchrotron Radiat. 8 (2001) 354.
[48] C.G. Schroer, M. Kuhlmann, U.T. Hunger, T.F. Günzler, O. Kurapova, S. Feste, F. Frehse, B. Lengeler, M. Drakopoulos, A. Somogyi, A.S. Simionovici, A. Snigirev, I. Snigireva, C. Schug, W.H. Schröder, Appl. Phys. Lett. 82 (2003) 1485.
[49] A.P.V. Soares, M.F. Portela, A. Kiennemann, Catal. Rev. Sci. Eng. 47 (2005) 125.
[50] A. Brückner, E. Kondratenko, Catal. Today 113 (2006) 16.
[51] G.W. Coulson, S.R. Bare, H. Kung, K. Birkeland, G.K. Bethke, R. Harlow, N. Herron, P.L. Lee, Science 275 (1997) 191.
[52] L. Basini, A. Guarinoni, A. Aragno, J. Catal. 190 (2000) 284.
[53] A.P.E. York, T.C. Xiao, M.L.H. Green, Top. Catal. 22 (2003) 345–358.
[54] Y.H. Hu, E. Ruckenstein, Adv. Catal. 48 (2004) 297.
[55] S. Pascarelli, T. Neisius, S. DePanfilis, J. Synchrotron Radiat. 6 (1999 1044).
[56] S. Hannemann, J.-D. Grunwaldt, N.v. Vegten, A. Baiker, P. Boye, C.G. Schroer, Catal. Today (2007) 54.
[57] S. Hannemann, J.-D. Grunwaldt, B. Kimmerle, A. Baiker, P. Boye, C.G. Schroer, Topics Catal., in press.
[58] R. Imbihl, G. Ertl, Chem. Rev. 95 (1995) 697.
[59] S. Nettesheim, A.v. Oertzen, H.H. Rotermund, G. Ertl, J. Phys. Chem. 98 (1993) 9977.
[60] A. Schneider, J. Mantzaras, S. Eriksson, Combust. Sci. Technol. 180 (2008) 89.
[61] L. Basini, M. Marchionna, A. Aragno, J. Phys. Chem. 96 (1992) 9431.

[62] J.-D. Grunwaldt, L. Basini, B.S. Clausen, J. Catal. 200 (2001) 321.
[63] P. Coan, A. Peterzol, S. Fiedler, C. Ponchut, J.-C. Labiche, A. Bravin, J. Synchrotron Radiat. 13 (2006) 260.
[64] J.-C. Labiche, O. Mathon, S. Pascarelli, M.A. Newton, G.G. Ferre, C. Curfs, G. Vaughan, A. Horns, D.F. Carreiras, Rev. Sci. Instrum. 78 (2007) 091301.
[65] B. Kimmerle, J.-D. Grunwaldt, A. Baiker, P. Glatzel, P. Boye, S. Stephan, C.G. Schroer, in preparation.
[66] T. Ressler, M. Hagelstein, U. Hatje, W. Metz, J. Phys. Chem. B 101 (1997) 6680.
[67] K. Proost, L. Vincze, K. Janssens, N. Gao, E. Bulska, M. Schreiner, G. Falkenberg, X-ray Spectrom. 32 (2003) 215.
[68] K. Proost, K. Janssens, B. Wagner, E. Bulska, M. Schreiner, Nucl. Instrum. Methods Phys. Res. B 213 (2004) 723.
[69] D. Vantelon, A. Lanzirotti, A.C. Scheinost, R. Kretzschmar, Environ. Sci. Technol. 39 (2005) 4808.
[70] N. Tsapatsaris, A.M. Beesley, N. Weiher, H. Tatton, A.J. Dent, F.J.W. Mosselmans, M. Tromp, S. Russu, J. Evans, I. Harvey, S. Hayama, S.L.M. Schroeder, AIP Conf. Proc. 882 (2007) 597.
[71] J.-D. Grunwaldt, B. Kimmerle, S. Hannemann, A. Baiker, P. Boye, C.G. Schroer, J. Mater. Chem. 17 (2007) 2603.
[72] B. Kimmerle, P. Haider, J.-D. Grunwaldt, A. Baiker, P. Boye, C.G. Schroer, Appl. Catal. A: Gen 353 (2009) 36–45.
[73] F.C. Moates, M. Somani, J. Annamalai, J.T. Richardson, D. Luss, R.C. Wilson, Ind. Eng. Chem. Res. 35 (1996) 4801.
[74] C.M. Snively, G. Oskarsdottir, J. Lauterbach, Catal. Today 67 (2001) 357.
[75] A. Holzwarth, H.-W. Schmidt, W.F. Maier, Angew. Chem. Int. Ed. 37 (1998) 2644.
[76] C.G. Schroer, P. Cloetens, M. Rivers, A. Snigirev, A. Takeuchi, W. Yun, MRS Bull. 29 (2004) 157.
[77] H. Mimura, S. Matsuyama, H. Yumoto, K. Yamamura, Y. Sano, M. Shibahara, K. Endo, Y. Mori, Y. Nishino, K. Tamasaku, M. Yabashi, T. Ishikawa, K. Yamauchi, Jpn. J. Appl. Phys. 44 (2005) L539.
[78] O. Hignette, P. Cloetens, G. Rostaing, P. Bernard, C. Morawe, Rev. Sci. Instrum. 76 (2005) 063709.
[79] C.G. Schroer, O. Kurapova, J. Patommel, P. Boye, J. Feldkamp, B. Lengeler, M. Burghammer, C. Riekel, L. Vincze, A. van der Hart, M. Küchler, Appl. Phys. Lett. 87 (2005) 124103.
[80] www.xradia.com.
[81] C.G. Schroer, B. Lengeler, Phys. Rev. Lett. 94 (2005) 054802.
[82] H.C. Kang, J. Maser, G.B. Stephenson, C. Liu, R. Conley, A.T. Macrander, S. Vogt, Phys. Rev. Lett. 96 (2006) 127401.
[83] C. Song, R. Bergstrom, D. Ramunno-Johnson, H. Jiang, D. Paterson, M.D.D. Jonge, I. McNulty, J. Lee, K.L. Wang, J. Miao, Phys. Rev. Lett. 100 (2008) 4.
[84] C.G. Schroer, P. Boye, J. Feldkamp, J. Patommel, A. Schropp, A. Schwab, S. Stephan, M. Burghammer, S. Schöder, C. Riekel, Phys. Rev. Lett. 101 (2008).
[85] J.-D. Grunwaldt, B. Kimmerle, P. Boye, C.G. Schroer, P. Glatzel, ESRF Spotlight, 2007. http://www.esrf.eu/news/spotlight/spotlight46/spotlight46/.
[86] R. Strobel, A. Baiker, S.E. Pratsinis, Adv. Powder Technol. 17 (2006) 457.
[87] A. Baiker, D. Gasser, J. Lenzner, A. Reller, R. Schlögl, J. Catal. 126 (1990) 555.
[88] J.-D. Grunwaldt, M. Maciejewski, A. Baiker, Phys. Chem. Chem. Phys. 5 (2003) 1481.